Ultrafast compound imaging for 2-D motion vector estimation: Application to transient elastography

Article *in* IEEE Transactions on Ultrasonics Ferroelectrics and Frequency Control · November 2002

DOI: 10.1109/TUFFC.2002.1041078 · Source: PubMed

4 authors, including:

Mickaël Tanter
École Supérieure de Physique et de Chimie Industrielles
595 PUBLICATIONS **17,163** CITATIONS

SEE PROFILE

Jeremy Bercoff
Supersonic Imagine
77 PUBLICATIONS **5,533** CITATIONS

SEE PROFILE

Laurent Sandrin
Echosens
103 PUBLICATIONS **4,593** CITATIONS

SEE PROFILE

Ultrafast Compound Imaging for 2-D Motion Vector Estimation: Application to Transient Elastography

Mickaël Tanter, Jeremy Bercoff, Laurent Sandrin, and Mathias Fink

***Abstract*—This paper describes a new technique for two-dimensional (2-D) imaging of the motion vector at a very high frame rate with ultrasound. Its potential is experimentally demonstrated for transient elastography. But, beyond this application, it also could be promising for color flow and reflectivity imaging. To date, only axial displacements induced in human tissues by low-frequency vibrators were measured during transient elastography. The proposed technique allows us to follow both axial and lateral displacements during the shear wave propagation and thus should improve Young's modulus image reconstruction. The process is a combination of several ideas well-known in ultrasonic imaging: ultra-fast imaging, multisynthetic aperture beamforming, 1-D speckle tracking, and compound imaging. Classical beamforming in the transmit mode is replaced here by a single plane wave insonification increasing the frame rate by at least a factor of 128. The beamforming is achieved only in the receive mode on two independent subapertures. Comparison of successive frames by a classical 1-D speckle tracking algorithm allows estimation of displacements along two different directions linked to the subapertures beams. The variance of the estimates is finally improved by tilting the emitting plane wave at each insonification, thus allowing reception of successive decorrelated speckle patterns.**

I. Introduction

By estimating motion induced in soft tissues by mechanical excitations, elastography became a wide area to study biological tissues elastic properties. Several ultrasound-based techniques have been developed according to the kind of excitation chosen: static compression [1], [2], dynamic vibrations [3]–[5], or pulsed excitations [6]–[10]. The work presented in this paper is based on the technique proposed by Catheline *et al.* [6], [7] and Sandrin *et al.* [8]–[10], called transient elastography, which consists in generating a pulsed low-frequency excitation at the surface of the soft tissue. This technique has the advantage to be insensitive to patient motion and boundaries conditions artifacts, because of its real-time capabilities (acquisition time of a few tens of milliseconds). The pulsed excitation induces a shear wave propagation in the tissues whose local velocity (typically from 1 to 10 m/s) is directly related to the local Young's modulus. Displacements induced in the media by the shear wave are measured with a single ultrasonic transducer connected to an ultrafast imaging system (up 6000 images/s), able to follow the shear wave propagation. This ultrafast frame rate is achieved by reducing the emitting mode to a single plane wave insonification and storing all backscattered RF data in memories. The beamforming process then is achieved in the receive mode during a postacquisition process. By using a 1-D cross correlation algorithm between successive images [11], [12], axial displacements induced in the medium are calculated at each time across the whole ultrasound image. Solving the inverse problem of the shear wave propagation on this axial component of the displacement allows us to deduce the Young's modulus image of the medium, as explained by Oliphant *et al.* [13].

Since today, the 1-D cross correlation algorithm measures only the ultrasound beam axis displacement component, giving only a partial recovery of the shear wave propagation. Static elastography shared the same problems, giving only the axial strain component estimation. Recently, Konafagou and Ophin [13] proposed a technique to recover the lateral displacements and strain. This kind of problem is recurrent in the ultrasound motion estimation field: pulsed Doppler and color flow mapping, implemented in ultrasound devices, are techniques measuring and displaying only the axial component of the blood or tissue velocity. Several techniques had already been proposed to estimate the lateral component (of displacement or velocity): geometric calculation using multiple beams from separate transducers [14], diffraction effects on the Doppler bandwidth widening [15], 2-D speckle tracking [16]–[19], and spatial quadrature [20], [21]. Recently the use of different subapertures from the same transducers was successfully implemented to achieve 2-D real-time velocity estimation in Doppler mode [22], [23].

In this paper, we propose a new technique, based on multisynthetic aperture beamforming, robust enough to estimate with a very high frame rate both axial and lateral displacements induced in the medium by the shear wave propagation. Indeed, the knowledge of the lateral displacement should help us to improve the Young's modulus reconstruction, especially providing data in areas in which the axial displacement is weak. The constraints imposed by our application are very important. A local estimation of small displacements (from 1 to 100 μm) over a large-scale image with a very high frame rate (up to 6000 frames.s^{-1}) is required. However, the beamforming does not need to be achieved in real time, and the great versatility of our ultrafast imaging system allows us to record all the RF data received on each transducer.

Manuscript received October 8, 2001; accepted April 9, 2002.

The authors are with the Laboratoire Ondes et Acoustique, ESPCI, Université Paris VII, U.M.R. C.N.R.S. 7587, 75005 Paris, France (e-mail: michael.tanter@espci.fr).

In Section II, the optimization of the multisynthetic aperture beamforming in the receive mode for displacement vector estimation is discussed. In particular, the influence of beam angles and subaperture sizes are discussed with experimental results. According to these results, we propose a new beamforming optimized for each local area of the image, resulting in a good estimation of the displacement vector in the whole ultrasound image.

In Section III, we show how the variance of the lateral displacement estimates can be improved by compounded plane wave insonifications. The application of compounding principles to real-time ultrasound imaging is not new [24], [25]; and, according to the substantial increasing of computational power on modern devices, real-time compounding was even recently implemented with success on commercial Philips Medical ultrasound systems [26]. We propose here to apply this compounding technique to our plane wave insonifications and combine it to multisynthetic aperture beamforming in the receive mode. As we will see, the improvement of motion estimates variance due to compounded insonifications is strongly enhanced here by an important decorrelation between successive compounded images resulting from the lack of transmit focusing.

In Section IV, the ability of our technique to produce very high frame rate images of the 2-D displacements vector is experimentally demonstrated on tissue mimicking phantoms for transient elastography. Its potential for flow measurements also is discussed briefly and will be detailed in further works. The insertion of the lateral displacement in the inverse problem processing of the shear wave propagation will be described in following works.

II. Multi Synthetic Aperture Beamforming

A. Device and Acquisition Sequence Description

To perform the ultrafast imaging, we developed a fully programmable multichannel system made of 128 channels connected to the transducers (Fig. 1). Each element possesses its own emission/reception electronic board, its own 2 Mbytes memory able to store successive emission and reception signals. All sequences of complex beamforming in the transmit and receive mode can be programmed and stored in a static RAM managing the real-time acquisitions. The ultrafast imaging is achieved by illuminating the medium with a plane wave at a pulse repetition varying between 500 and 6000 Hz (Fig. 2). All backscattered RF echoes are stored in the 2 Mbytes memory of each transducer and transmitted in the computer after the acquisition. A typical maximum number of 200–300 RF datasets ($\sim$6 cm depth) can be acquired in a complete acquisition sequence.

B. Measurement of the Axial and Lateral Displacements

The vector motion can be estimated easily in two dimensions by using separate subapertures in the receive beamforming process (Fig. 3). The measurement of the motion along two different directions is performed here by using a plane wave insonification T_x on whole array in the transmit mode and two lateral subapertures, R_{x1} and R_{x2}, in the receive mode. The plane wave transmitted has a 0° angle steering ($\vec{u}_0$ in Fig. 3); the two subapertures, R_{x1} and R_{x2}, have different steering angles α_0 and α_1. Thus, for each plane wave insonification, we perform two different speckle images (right and left) corresponding, respectively, to the right and left subapertures used during the receive beamforming process. The beamforming process in the receive mode simply consists in delaying the backscattered echoes received on each transducer of the two subapertures with a classical cylindrical time delay law and finally summing the delayed contributions of each transducer of the subaperture. This cylindrical time-delay law consists in calculating the different times of flight between each transducer and the desired focal point.

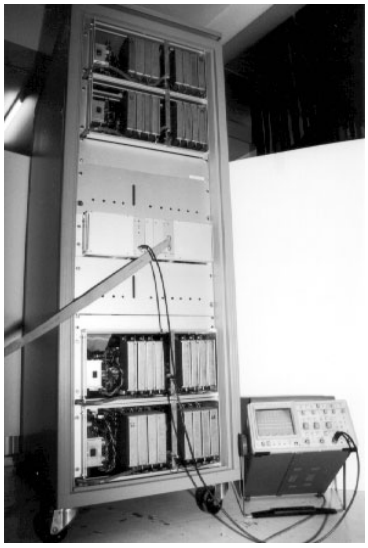

Fig. 1. Ultrafast multichannel system made of 128 fully programmable emission/reception electronic channels.

The vector displacement occurring between two plane wave insonifications is estimated by implementing a classical speckle tracking technique (1-D cross-correlation algorithm) on successive speckle images (i.e., two successive left images and two successive right images) (Fig. 3). At a given depth Z_0 on the j^{th} line, the 1-D cross-correlation algorithm allows one to estimate two different time delays, $t_{\alpha 0}$ and $t_{\alpha 1}$. It can be shown, using a plane wave decomposition, that each of these time delays corresponds to the sum of the projections of the displacement vector $\vec{d}(dx, dz)$ along the incident beam axis and the receiving beam direction:

$$t_{\alpha_0} = \frac{dz + dz\cos\alpha_0 + dx\sin\alpha_0}{c}, \qquad t_{\alpha_1} = \frac{dz + dz\cos\alpha_1 + dx\sin\alpha_1}{c}. \tag{1}$$

Note that α_0 and α_1 are known as they only depend on geometrical parameters (focal length, subaperture position, and width). Thus, the axial and lateral displacements

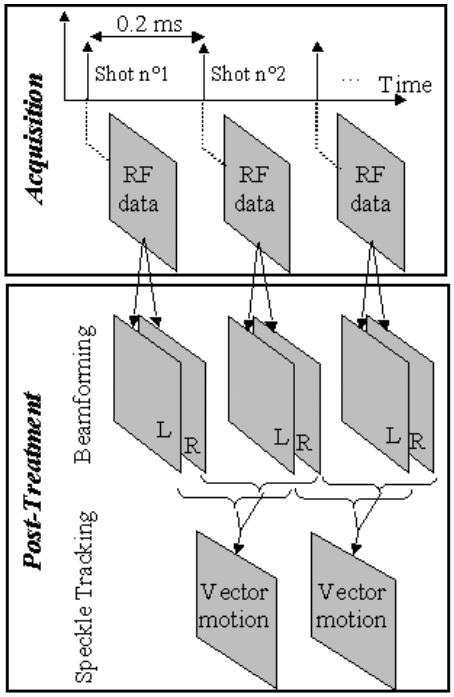

Fig. 2. Acquisition and post-treatment processing. Up to 5000 plane wave emissions are achieved per second. All backscattered echoes are recorded in each RAM memory dedicated to each element. The beamforming is achieved in post-treatment allowing production for each insonification both left and right speckle images. The 1-D cross correlations between successive images lead to the motion vector image at each time.

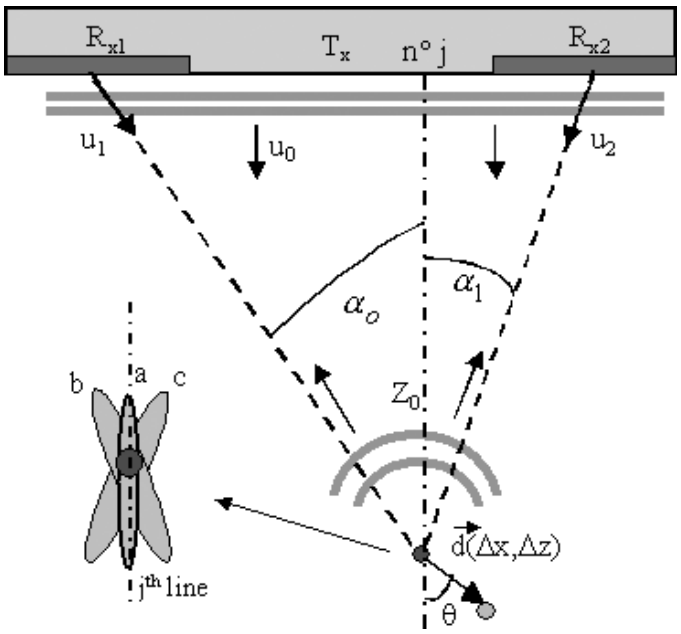

Fig. 3. Left and right subapertures performing two different left and right speckle images. The focal spot allowing one to perform a segment (at depth Z_0) of the j^{th} line of the image is presented: (a) for a classical transmit-receive beamforming, (b) for the left subaperture receive beamforming, (c) for the right subaperture receive beamforming.

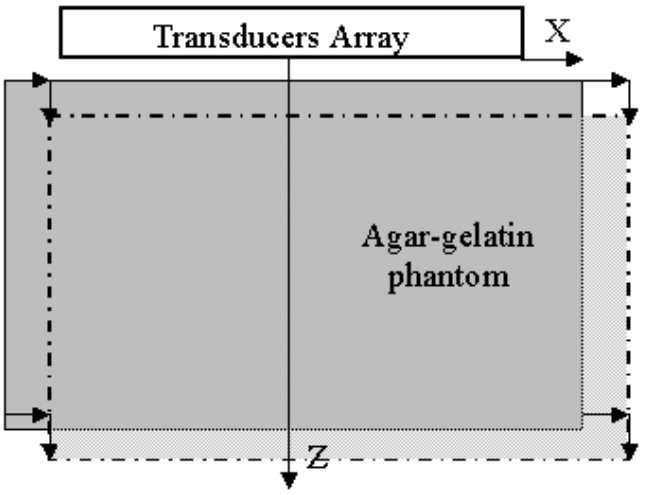

Fig. 4. Experiment in an agar-gelatin phantom: 50 μm axial and lateral displacement.

can be deduced easily from the knowledge of $t_{\alpha 0}$ and $t_{\alpha 1}$:

$$dz = \frac{ct_{\alpha_0}\sin\alpha_1 + ct_{\alpha_1}\sin\alpha_0}{(1+\cos\alpha_0)\sin\alpha_1 - (1+\cos\alpha_1)\sin\alpha_0},$$
$$dx = \frac{ct_{\alpha_1}(1+\cos\alpha_0) - ct_{\alpha_0}(1+\cos\alpha_1)}{(1+\cos\alpha_0)\sin\alpha_1 - (1+\cos\alpha_1)\sin\alpha_0}. \quad (2)$$

One can notice that we find back the analogy to vector Doppler estimation [14] in the particular case of $\alpha_0 = -\alpha_1$:

$$dz = \frac{ct_{\alpha_0} + ct_{\alpha_1}}{2(1+\cos\alpha_0)},$$
$$dx = \frac{ct_{\alpha_1} - ct_{\alpha_0}}{2\sin\alpha_0}. \quad (3)$$

As described in Section II-D, the steering angle between the two subapertures must be chosen as the maximum available angle in order to maximize the accuracy of the vector displacement estimation.

C. Experimental Validation and Transducer Directivity Influence

A first experiment is achieved in an agar-gelatin phantom (Fig. 4). An initial plane wave insonification is emitted by the array, and the backscattered echoes are beamformed over the two subapertures to produce the two first left and right speckle images. Then the phantom is manually moved 50 μm along the x direction and 50 μm along the z direction. A second plane wave insonification then is achieved, and the backscattered echoes are used to process the final left and right speckle images. In this first in vitro experiment, we used the same subapertures to process each line and each depth of the left and right speckle images (Fig. 5).

Fig. 6 presents the two initial images of the phantom (before displacement) achieved, respectively, with the left and right subapertures. Symmetric shadow areas appear on each image due to the directivity of the array elements.

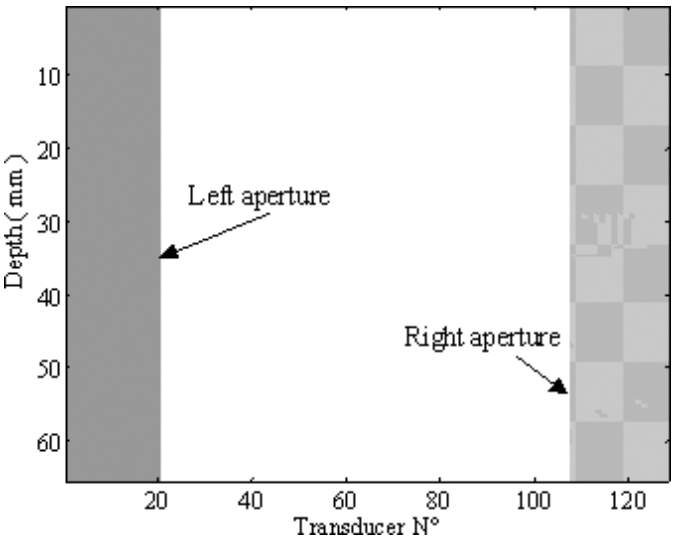

Fig. 5. Active elements of the array versus focal depth in the receive beamforming mode.

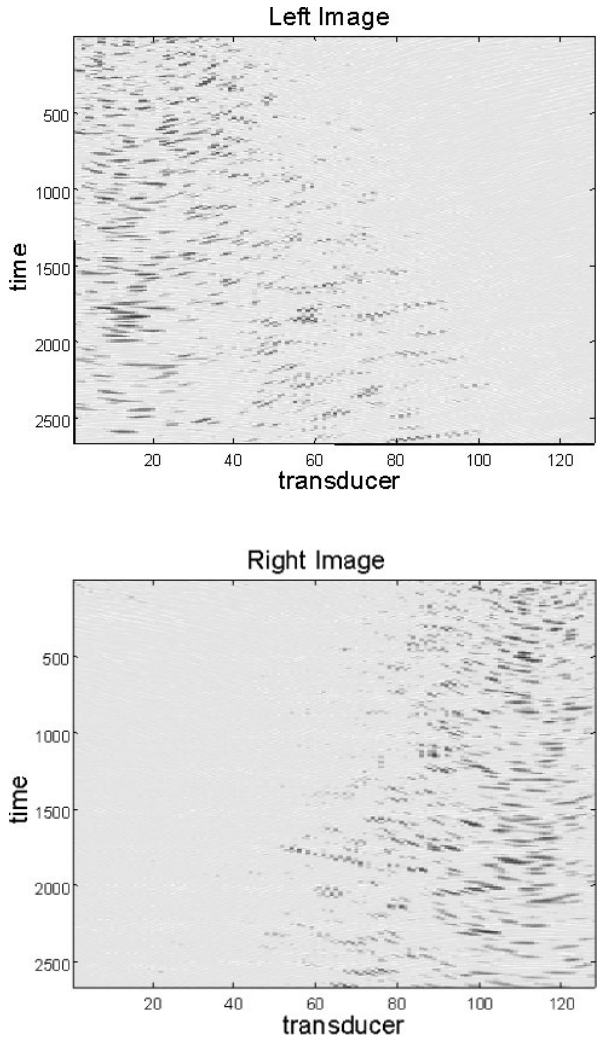

Fig. 6. Speckle images of the phantom achieved, respectively, with the left and right subapertures defined in Fig. 4. Directivity limits of the transducer elements appears clearly in the images.

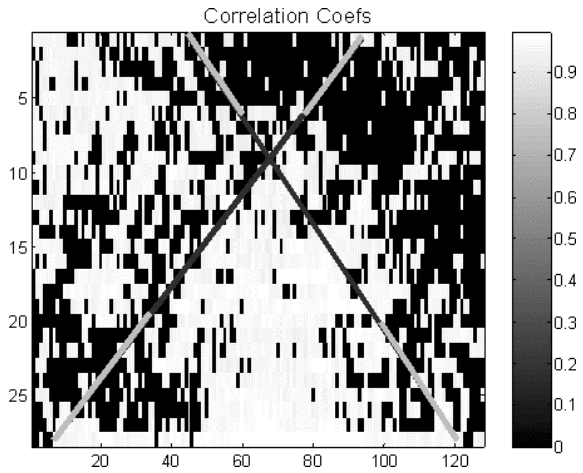

Fig. 7. Mean of the left and right correlation coefficients. The white curves approximately correspond to the directivity pattern involved by the elements of the left and right subapertures. One could think that a larger estimation area could be inspected by increasing the subapertures width. However, increasing the subaperture width results in a decreasing of α_0 and α_1 and, as explained, a beam angle decreasing lead to a dramatic increasing of the estimates variance.

These two images are compared using a classical 1-D cross-correlation technique with the two corresponding images achieved after phantom displacement. Fig. 7 presents the mean of the correlation coefficients obtained for both left and right images, describing the spatial mapping of the displacement estimation quality [27]. As one can notice, this mean of left and right correlation coefficients is higher than 0.9 only in a restricted conic area. This area corresponds to the cross intersection between the directivity patterns of elements of the right and left subapertures. The estimation of $t_{\alpha 0}$ and $t_{\alpha 1}$ is achieved by using 1-D speckle tracking [8], [9] windows of about 10 wavelengths (corresponding to a 1.5 mm depth window at our 50 MHz sampling frequency) with a 50% overlap. According to (2), we deduce dx and dz at each speckle tracking window location (Fig. 8). Displacements of 50 microns along x and z axis are measured with good accuracy inside the common zone of the two directivity patterns.

D. Beam Angle Dependence

In order to study the estimates variance dependence on the beam angles, the same in vitro experiment was realized with a new beamforming (Fig. 9). The subapertures used in the construction of each line of the image are different at each depth. They were computed to ensure a constant beam angle α_0 and a constant f-number (ratio between the focal length and the array aperture) factor at each depth on the central line of the image (Fig. 9). Longitudinal and lateral displacements then are deduced from (2), and the variance of the vector displacement estimation is calculated over a limited area of the image [blank rectangle on Fig. 8(a)].

This vector displacement variance measurement is achieved several times by using different constant angles

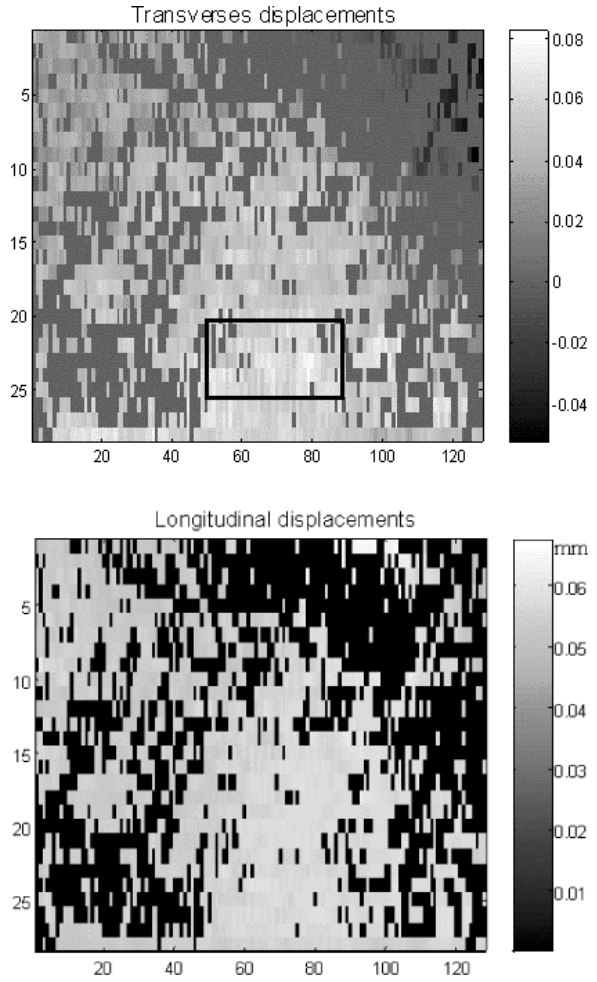

Fig. 8. (a) Longitudinal and (b) lateral displacements estimates in millimeters.

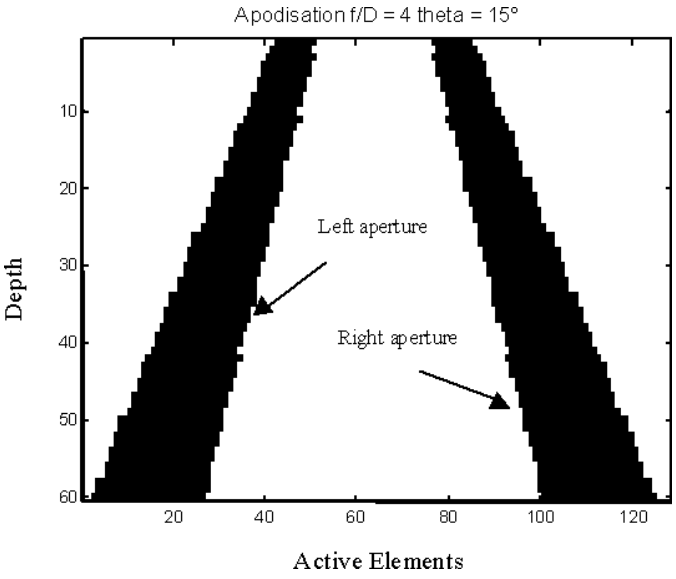

Fig. 9. Beamforming apodization used along the central line of the image. For each depth, black lines indicate the active elements of the array in the receive beamforming mode for the left and the right subaperture. The size of both subaperture are chosen to ensure a constant beam angle and a constant F/D factor at each depth.

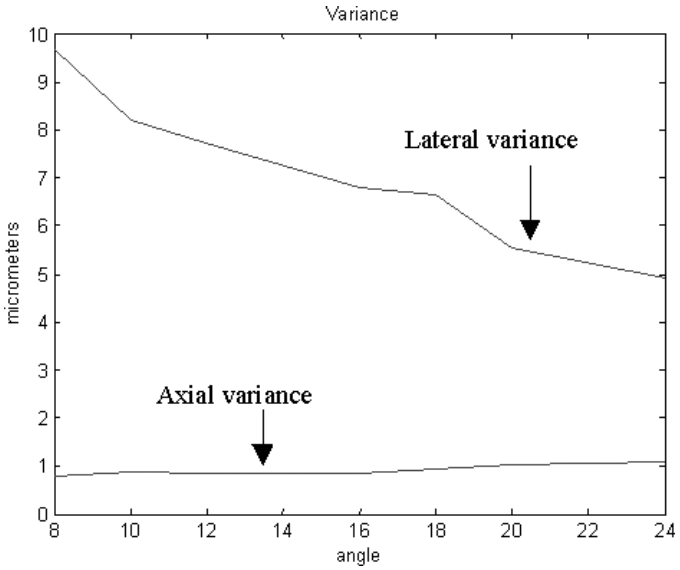

Fig. 10. Dependence of the lateral and longitudinal displacements variance with the angle between subapertures (in degrees). For a 50-μm displacement applied in both directions, the mean estimate of the lateral and longitudinal displacements are, respectively, 48 and 51 μm.

α_0 for the beamforming process. The dependence of the estimates variance on the beam angle α_0 is presented on Fig. 10. Although the axial displacement variance does not depend on the beam angle, the variance of the lateral displacement estimates clearly decreases as long as the beam angle increases[1]. Unfortunately, at maximal depths, a typical angle of 24° cannot be overcome without decreasing the subaperture width and reducing the spatial resolution of the focal spot. Moreover, increasing the angle too much will strongly decrease the size of the cross area allowing good left and right correlation coefficients. Thus, one can notice that the transducer directivity is an important parameter, and a $\lambda/2$ pitch transducer array would be more appropriate for such lateral estimation.

E. Line and Depth Adapted Beamforming

In order to measure the vector displacements over the widest area of the echographic image, a different pair of subapertures are used for each depth and for each line of the image during the receive beamforming process. For each line of the image, the two subapertures are chosen to be symmetrical with regard to the line position [Fig. 11(c)]. This symmetry is kept as long as the subapertures do not reach the image lateral boundaries. For construction of near-edges lines, subapertures are chosen to approach at best this symmetry while remaining in the array aperture [Figs. 11(a, b, and d)].

As an immediate result, this beamforming, matched to each speckle tracking location, produces very good left and

[1]This can be shown by deriving the relative error made on axial and lateral displacements dx and dz [see (2)] regarding small variations of the beam angle α_0.

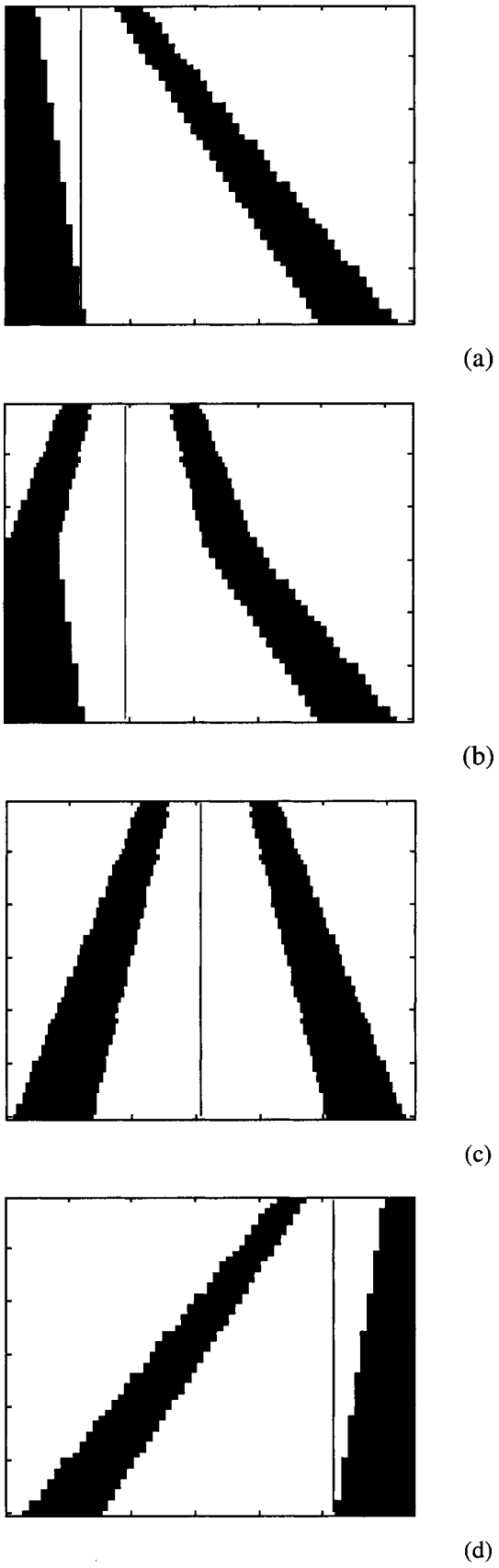

Fig. 11. Line and depth matched beamforming: left and right subapertures used to process the beamforming in the receive mode (a) for line no. 20, (b) for line no. 40, (c) for line no. 64, and (d) for line no. 100.

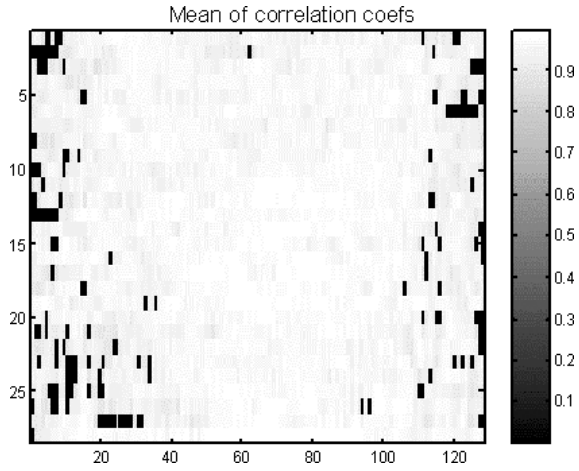

Fig. 12. Mean of the left and right correlation coefficients obtained by 1-D speckle tracking between left and right images achieved with the line and depth matched beamforming defined in Fig. 9.

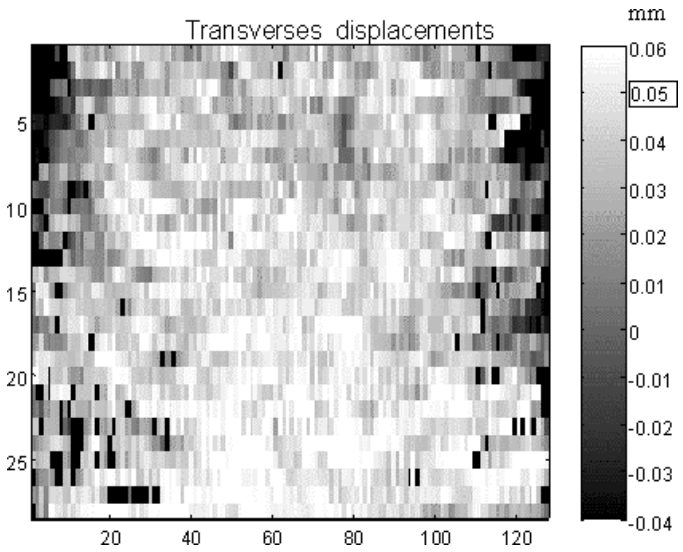

Fig. 13. Image of the lateral displacement (in millimeters) of the phantom achieved by using the line and depth matched beamforming.

right correlation coefficients over almost the whole image. The mean of the left and right correlation coefficients is presented on Fig. 12. The corresponding lateral displacements estimates are presented on Fig. 13. Except on the edges of the image, the 50 μm lateral displacement of the phantom is properly estimated (i.e., with a variance below 10 microns). We remind the reader here that these measurements were achieved by illuminating the medium only two times with a plane wave: one insonification before and one after the phantom displacement. However, averaging the vector displacement estimation over several identical acquisitions did not decrease the variance of the measurements. This experimental result is explained by the fact that the speckle pattern remains unchanged from one acquisition to the next one.

III. Ultrafast Compounding

A. Principle

In order to decrease the variance of our lateral displacement measurements, we propose to introduce sequences of N successive compounded plane waves insonification (Fig. 14). The aim is to produce, for each insonification, new decorrelated RF data. The beamforming process then is applied in the receive mode as described in Section II-E. Thus, for each plane wave insonification at a different angle, two speckle images (left and right) are processed. The displacement vector is then estimated by using the 1-D cross correlation between speckle images corresponding to plane wave insonifications of the same angles (i.e., between $t = T_i$ and $t = T_{i+N+1}$, $t = T_{i+1}$ and $t = T_{i+N+2}$, $t = T_{i+2}$ and $t = T_{i+N+3}$, Fig. 14). These vector displacements are averaged over the number N of different consecutive emission angles.

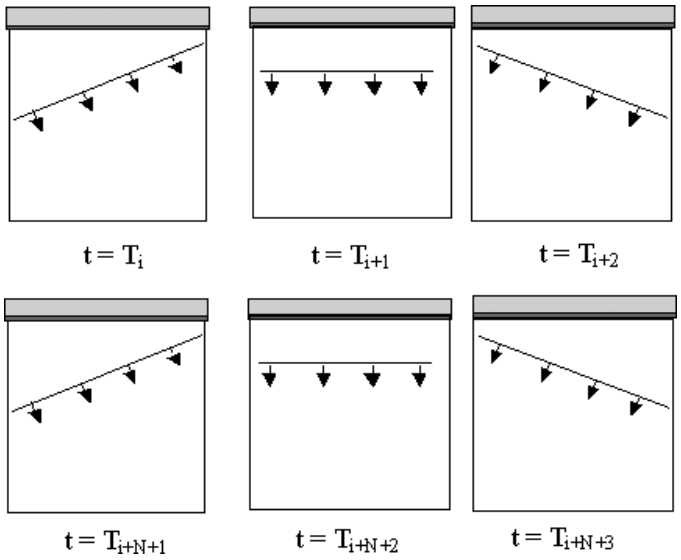

Fig. 14. Sequence of successive compounded plane wave insonifications. In this case, N = 3.

B. Improvement of the Estimates Variance

This new emission process is applied to the test experiment presented in Fig. 4. A finite number N of compounded plane waves is successively emitted, and the backscattered echoes are stored in a part of the channel memories. Then the phantom is moved 50 μm laterally and axially, as shown in Fig. 3, and a new set of N compounded plane wave insonifications is achieved. The resulting backscattered echoes also are stored in the channel memories. After estimation of the vector displacements between emissions of identically tilted plane waves, the measurements are averaged over N. Fig. 15(a) presents the lateral displacements estimated by averaging over 11 different emission angles (tilting of $-10°$, $-8°$, $-6°$, $-4°$, $-2°$, $0°$, $2°$, $4°$, $6°$, $8°$, and $10°$). Fig. 15(b) presents a refined area of this image and can be compared to the lateral displacements estimated with only one emission angle, Fig. 15(c). As one can notice, the variance of the lateral displacement is strongly decreased by applying the emission compound process.

Fig. 16 presents the evolution of the variance [calculated in Fig. 15(b)] regarding the number N of averaged emission angles. The variance is clearly a decreasing function of N, which variations are very close to $\frac{1}{\sqrt{N}}$. The measurement of the transverse component reaches a 3 μm precision. These results can be explained by theoretical considerations. According to the Van Cittert Zernike theorem [28], [29], speckle patterns corresponding to different plane wave insonifications are strongly decorrelated as there is no transmit focusing. Indeed, the spatial coherence of ultrasonic speckle, described by the spatial autocorrelation function of the wavefield, is equal to the spatial Fourier transform of the source distribution. After a plane wave insonification, the backscattering source (i.e., scatterers in tissues) is widely spread in space. So, the Fourier transform of its spatial distribution presents a narrow shape, and the ultrasonic speckle is spatially more incoherent than for a focused transmission. Thus, our approach maximizes the benefit of the compound technique.

To illustrate this idea, the degree of similarity between two images of the same medium insonified by plane waves of different angles can be described by the correlation coefficients between corresponding line segments of these images. Note that these images are computed with the same receive beamforming. Fig. 17(a) presents the spatial map of the correlation coefficients between two different neighboring plane wave angles ($0°$ and $2°$). Fig. 17(b) is the spatial map for two distant angles ($0°$ and $10°$). Fig. 17(c) presents the evolution of the mean of the correlation coefficient across the whole map as the insonification angle increases from $-10°$ to $10°$ (with an interval of $2°$). The reference image is the one computed with a $-10°$ insonification.

There is a clear decorrelation increasing with the tilting angle. Thus, we can rely on independent speckle patterns allowing to build a more robust statistical estimator of the motion vector. However, the number N of plane wave insonification angles cannot be increased indefinitely. First, the edges of the image are not insonified when the plane wave emission angles become important, resulting in a decreasing of the estimation area [this is shown on Fig. 17(a)]. Second, averaging over a number N of emission angles decreases true frame rate by a factor N.

IV. Real-Time Acquisitions: Application to Transient Elastography

In this section, the goal is to follow the vector displacements induced in a soft tissue by a transient shear wave propagation. This will allow us to recover a 2-D image of the Young's modulus of the medium. Experimental acquisitions achieved on tissue mimicking phantoms

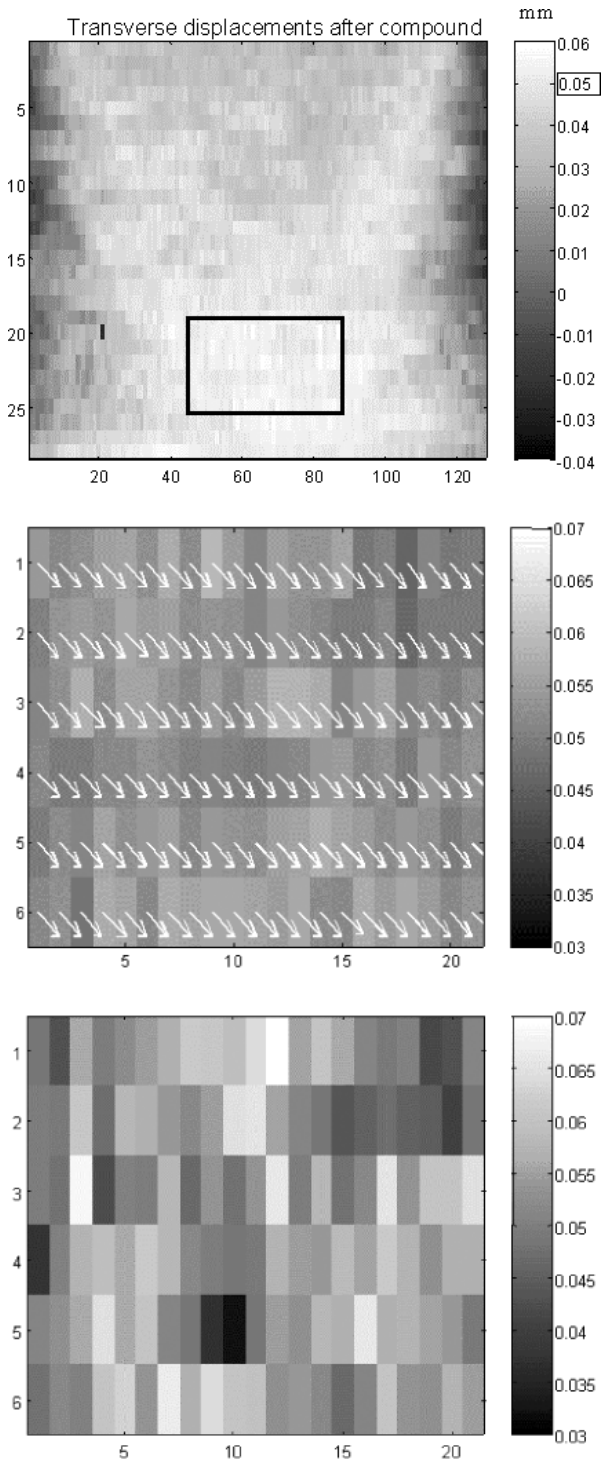

Fig. 15. a) Lateral displacements (in millimeters) estimated by using N = 11 different emission angles. (b) Detail of the image corresponding to the blank rectangle. (c) Lateral displacement in the same detailed area achieved by using only N = 1 emission angle. Arrows in (b) represent the corresponding vector displacements.

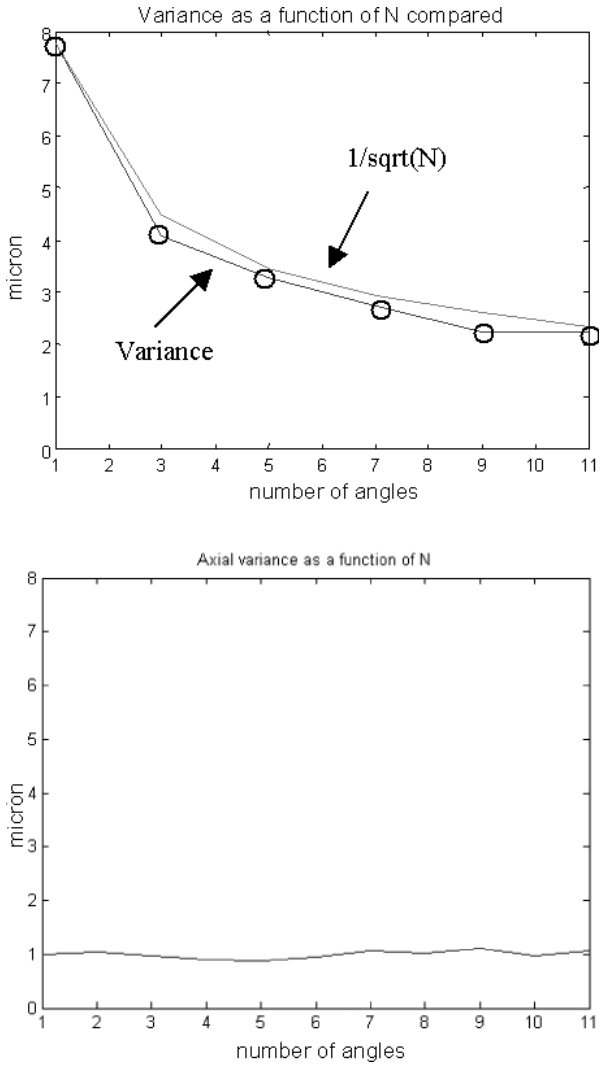

Fig. 16. Evolution of the estimates variance of the transverse displacement (first image) and the axial displacement with the number of averaged emission angles.

are described and discussed. In transient elastography, one should notice that shear waves are propagating in human tissues at typical frequencies of 50 Hz (50 Hz in soft tissues, 100 Hz in muscle) and inducing local particle velocities of a few millimeters per second. These are significantly lower than flow velocities in medical ultrasound flow imaging. However, in transient elastography, the particle velocities map evolves quickly in time and so need to be imaged with a much higher frame rate: the shear wave propagates at typical velocities of a few meters per second. On the contrary, the frame rate is not a crucial parameter in blood flow imaging, considering that the characteristic evolution time corresponds to a tenth of a cardiac rate (approximately a second); consequently, imaging blood flow at classical ultrasound system frame rate (50 Hz) is relevant, but results in a nonstrictly instantaneous velocity map. In other words, particle velocities are smaller in transient elastography than in flow imaging, but the time variations of these particle velocities are more important in elastography than in flow measurements. As we will see in Sec-

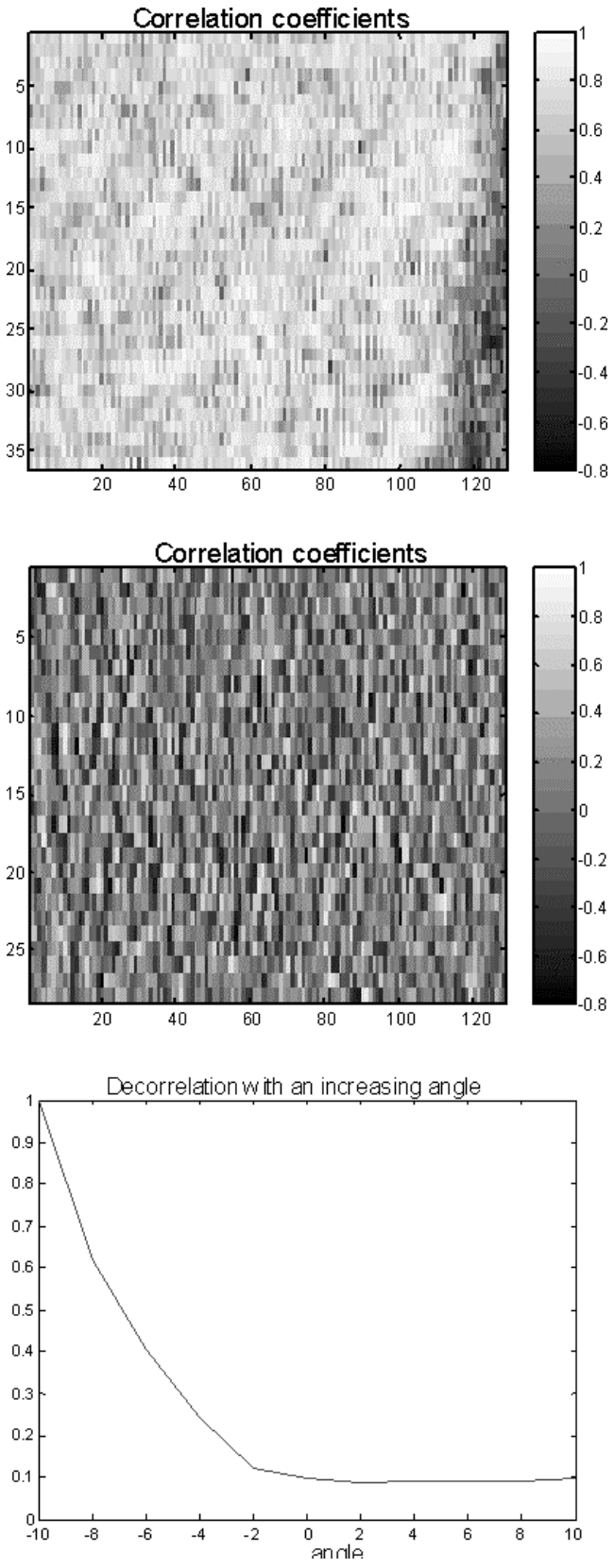

Fig. 17. (a) Correlation coefficients map achieved with two images of the same medium computed after a 10 and an 8 degrees insonification. (b) On the left, the same map with a 10 and a 0 degree insonifications. (c) Mean of the correlation coefficients calculated with images resulting from plane wave insonifications.

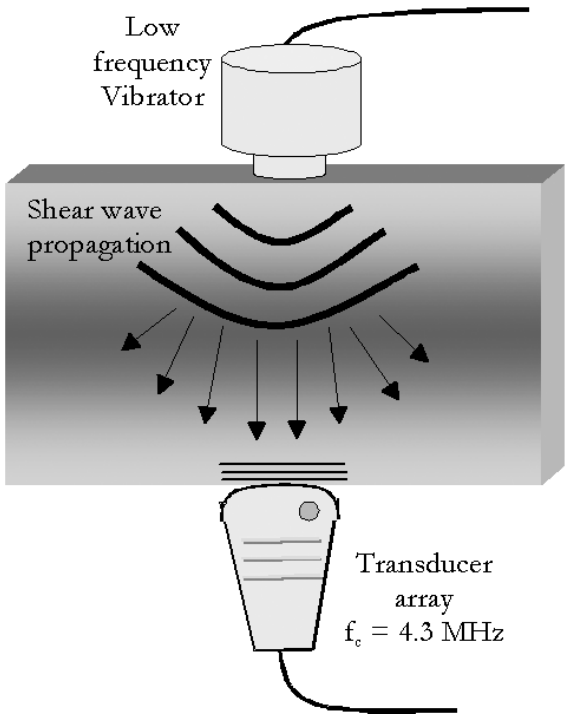

Fig. 18. Experimental setup.

tion III-C, these differences should induce slight modifications of the emission-reception sequencing process between both applications.

A. Experimental Setup and Real-Time Sequence

The experimental setup is presented on Fig. 18: an 8-mm diameter, low-frequency vibrator and a 128 transducers array are located on both sides of an Agar gelatin phantom. The ultrasonic array is working at a central frequency of 4.3 MHz, and the low-frequency vibrator generates a two-cycle pulse at a central frequency of 50 Hz. The array illuminates the medium with plane waves at a 5000 Hz repetition rate. Sets of $N = 11$ different plane wave angles are recursively emitted every 0.2 ms (Fig. 19). The vector displacements then are averaged over N successive estimates. This averaging is performed by using a temporal sliding window as described at the bottom of Fig. 19. Thus, it allows estimation of an averaged displacement without losing the initial frame rate, fr = 5000 Hz. Nevertheless, averaging over N successive displacements results in a temporal low-pass filtering (frequency cut off fr/N). This filter has a negligible effect at our frequency shear vibration. Increasing this frequency would require reducing the number N of averaging samples.

B. Results

A complete imaging sequence (described in Section III-A) made of 250 plane wave insonifications, is achieved with a 5000 Hz repetition rate while generating a 50 Hz transient vibration at the surface of the phantom. Fig. 20

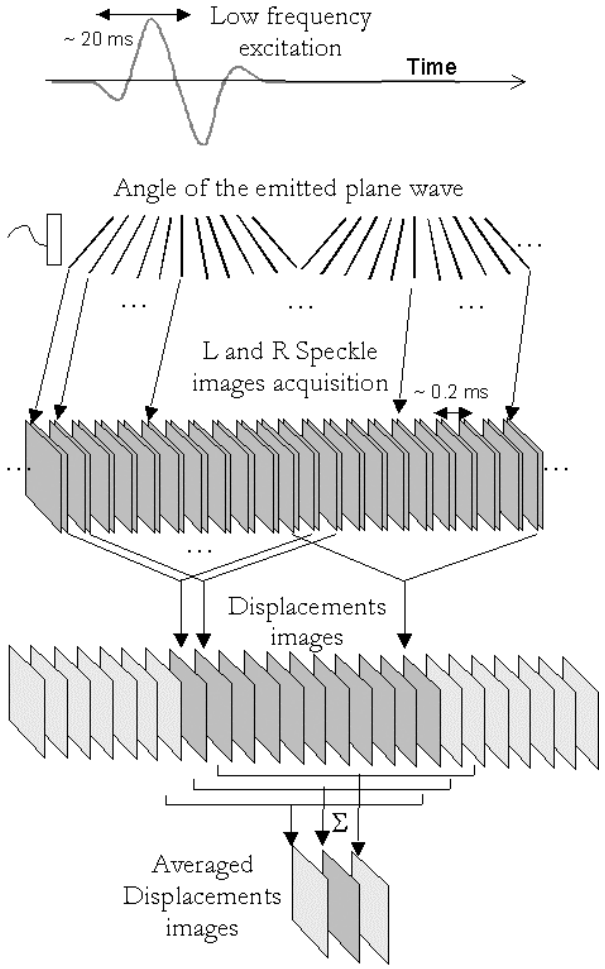

Fig. 19. The sequence of ultrafast compound imaging for 2-D vector displacements estimation: while the low-frequency vibrator generates a two cycles pulse (f ∼ 50 Hz), compounded ultrasonic plane waves are emitted by the transducer array at a repetition rate of 5000 Hz. N different tilt angles are emitted (here N = 11). The backscattered echoes are beamformed in the receive mode to produce two images (left and right). The 1-D cross correlation between L and R speckle images generated with the same emission angle allows one to deduce a 2-D image of the vector displacement every 1/5000 second. These images are averaged over the number N of different plane wave insonification angles. The averaging is made by using a sliding temporal window and thus allows one to preserve the initial 5000 Hz frame rate.

presents the axial and lateral displacements induced in the medium by the low-frequency pulsed vibrator. Due to symmetry considerations, one clearly recognizes the symmetrical and antisymmetrical behavior of the respective axial and lateral displacements. This experiment demonstrates the ability of this technique to follow the shear wave propagation in soft tissues as it is possible to image the 2-D displacement vector components of the soft medium over a large image plane (50 mm × 50 mm) during the propagation.

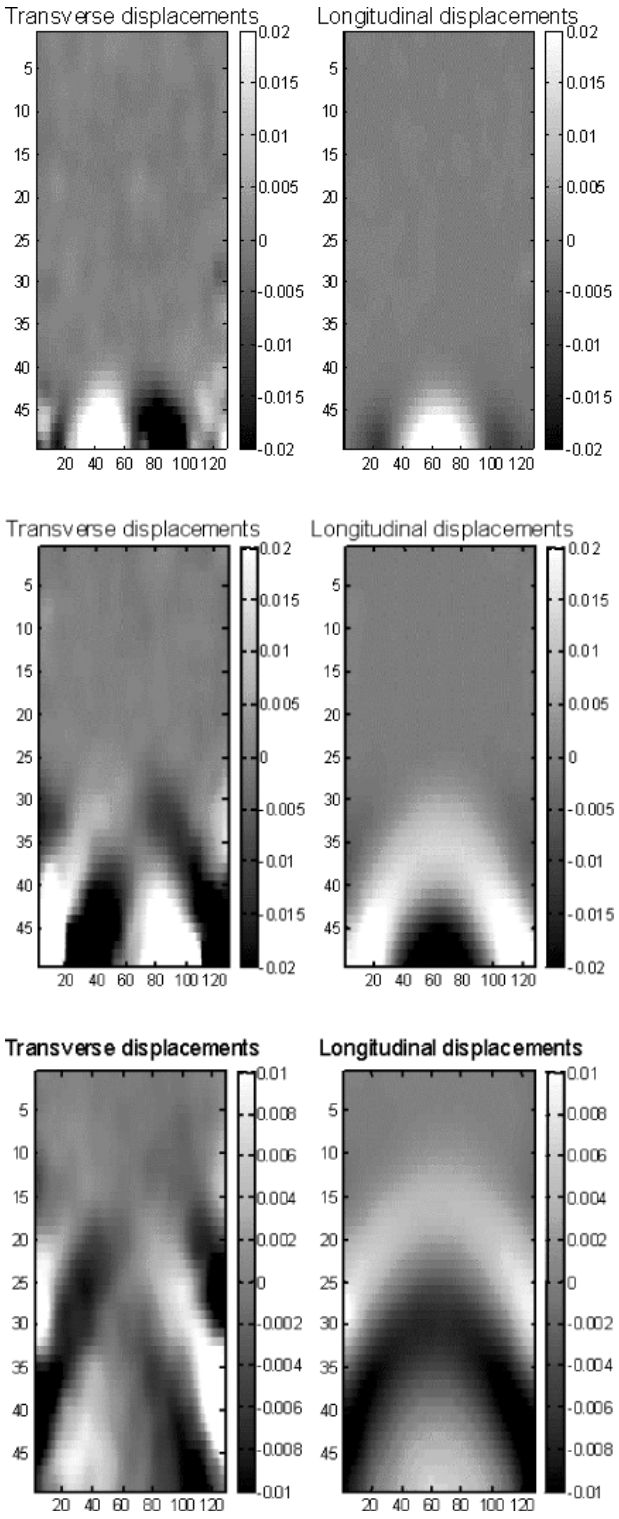

Fig. 20. Axial and lateral displacements induced in the phantom by the low-frequency transient vibration (located at the bottom of the image) at successive times. The resulting shear wave propagates at about 1 m.s^{-1} inside the medium.

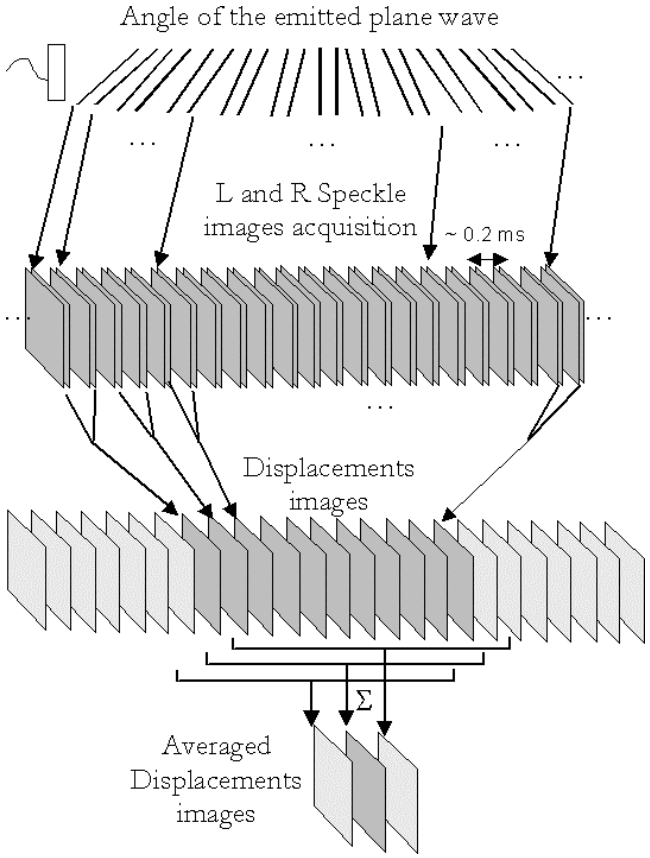

Fig. 21. Modification of the plane wave insonification sequences and displacement estimation processes for color flow imaging (to be compared with Fig. 15).

C. Emission Sequence Modification for Flow Measurements

Particle velocities are smaller in transient elastography than in flow imaging. So the tissue displacement due to the shear wave propagation is small between two successive speckle images acquired at a very high frame rate of 5000 Hz. Thus, the 1-D speckle tracking algorithm for local displacements measurement can be applied between speckle images separated by several plane wave insonifications (here $N = 11$). Nevertheless, the frame rate must remain important as the time variations of the tissue displacement are important (as they are related to the shear wave speed reaching, in some cases, more than 5 m per second). That is why the emission/reception sequencing process presented in Fig. 19 is particularly well adapted to the transient elastography application.

V. Summary and Conclusions

In blood flow imaging, the velocities to be measured are really higher than in transient elastography (about 20 cm.s^{-1}). The 1-D speckle tracking algorithm then should be applied between successive speckle images. The emission sequencing and displacement estimation processes should be modified in the way presented on Fig. 21. In that case, the 2-D displacement vector frame rate is divided by two in comparison with the pulse repetition, but this frame rate remains very high in comparison with classical Doppler frame rates. This sequencing process will be applied in further works to experimental flow measurements following previous investigations [30], [31].

Experiments made on tissue mimicking homogeneous phantoms validate the potential of this new ultra-fast, 2-D motion vector imaging technique for ultrasound-based transient elastography. Optimizing the subapertures size and location for each line beamforming in the receive mode allowed us to estimate motion vectors in a large area of the echographic image (optimal measurements were made with at least a 16° angle between the two apertures). Compounding plane waves in the transmit mode allows one to improve the accuracy and variance of lateral motion estimation without degrading the ultra-fast frame rate that is an essential parameter for transient elastography application. Very small displacements are detectable (up to 1.5 μm and 3 μm, respectively), for the axial and lateral displacements. The knowledge of both axial and lateral displacements in the image plane should improve the inverse problem solving especially in areas in which the axial displacement is lower than the transverse one. This issue will be discussed in further works. Beyond transient elastography applications, this technique could be of great interest for complex flows (e.g., turbulence, jet flow) imaging. The combination of the compounding technique with plane wave insonifications also could have promising applications in classical reflectivity imaging.

References

[1] J. Ophir, E. I. Cespedes, H. Ponnekanti, Y. Yazdi, and X. Li, "Elastography: A method for imaging the elasticity in biological tissues," *Ultrason. Imag.*, vol. 13, pp. 111–134, 1991.

[2] E. Konafagou and J. Ophir, "A new elastographic method for estimation and imaging of lateral displacement, lateral strains, corrected axial strains and Poisson's ratios in tissues," *Ultrasound Med. Biol.*, vol. 24, no. 8, pp. 1183–1199, 1998.

[3] R. M. Lerner, K. J. Parker, J. Holen, R. Gramiak, and R. C. Waag, "Sono-elasticity: Medical elasticity images derived from ultrasound signals in mechanically vibrated targets," *Acoust. Imaging*, vol. 16, pp. 317–327, 1987.

[4] Y. Yamakoshi, J. Sato, and T. Sato, "Ultrasonic imaging of internal vibration of soft tissue under forced vibration," *IEEE Trans. Ultrason., Ferroelect., Freq. Contr.*, vol. 37, no. 2, pp. 45–53, Mar. 1990.

[5] V. Dutt, R. R. Kinnick, and J. F. Greenleaf, "Acoustic shear wave displacement measurement using ultrasound," in *Proc. IEEE Ultrason. Symp.*, 1996, pp. 1185–1188.

[6] S. Catheline, F. Wu, and M. Fink, "A solution to diffraction biases in sonoelasticity: The acoustic impulse technique," *J. Acoust. Soc. Amer.*, vol. 105, pp. 2941–2950, May 1999.

[7] S. Catheline, J.-L. Thomas, F. Wu, and M. Fink, "Diffraction field of a low frequency vibrator in soft tissues using transient elastography," *IEEE Trans. Ultrason., Ferroelect., Freq. Contr.*, vol. 46, no. 4, pp. 1013–1019, 1999.

[8] L. Sandrin, S. Catheline, M. Tanter, X. Hennequin, and M. Fink, "Time-resolved pulsed elastography with ultrafast ultrasonic imaging," *Ultrason. Imag.*, vol. 21, pp. 259–270, 1999.

[9] L. Sandrin, M. Tanter, S. Catheline, and M. Fink, "Shear modulus imaging with time resolved 2-D pulsed elastography," *IEEE Trans. Ultrason., Ferroelect., Freq. Contr.*, vol. 49, pp. 426–435, Apr. 2002.

[10] L. Sandrin, M. Tanter, S. Catheline, and M. Fink, "Shear elasticity probe for soft tissues with time resolved 1-D pulsed elastography," *IEEE Trans. Ultrason., Ferroelect., Freq. Contr.*, vol. 49, no. 4, pp. 436–446, Apr. 2002.

[11] O. Bonnefous, P. Pesque, and X. Bernard, "A new velocity estimator for color flow mapping," *Proc. IEEE Ultrason. Symp.*, 1986, pp. 855–860.

[12] R. J. Dinckinson and C. R. Hill, "Measurement of soft tissue motion using correlation between A-scans," *Ultrasound Med. Biol.*, vol. 8, pp. 263–271, 1982.

[13] T. E. Oliphant, R. R. Kinnick, A. Manduca, R. L. Ehman, and J. F. Greenleaf, "An error analysis of Helmholtz inversion for incompressible shear, vibration elastography with application to filter-design for tissue characterization," in *Proc. IEEE Ultrason. Symp.*, 2000, pp. 1795–1798.

[14] M. D. Fox, "Multiple crossed-beam ultrasound Doppler velocimetry," *IEEE Trans. Sonics Ultrason.*, vol. 25, pp. 281–286, 1978.

[15] V. L. Newhouse, D. Censor, T. Vontz, J. A. Cisneros, and B. B. Goldberg, "Ultrasound Doppler probing of flows transverse with respect to beam axis," *IEEE Trans. Biomed. Eng.*, vol. 34, pp. 779–788, 1987.

[16] I. A. Hein and W. D. O'Brien, "Current time-domain methods for assessing tissue motion by analysis from reflected ultrasound echoes: A review," *IEEE Trans. Ultrason., Ferroelect., Freq. Contr.*, vol. 40, pp. 84–102, Mar. 1993.

[17] L. N. Bohs, B. H. Friemel, and G. E. Trahey, "Experimental velocity profiles and volumetric flow via two-dimensional speckle tracking," *Ultrasound Med. Biol.*, vol. 21, pp. 885–898, 1995.

[18] L. N. Bohs, B. J. Geiman, M. E. Anderson, S. M. Breit, and G. E. Trahey, "Ensemble tracking for 2-D vector velocity measurement: Experimental and initial clinical results," *IEEE Trans. Ultrason., Ferroelect., Freq. Contr.*, vol. 45, pp. 912–924, Jul. 1998.

[19] L. N. Bohs, B. J. Geiman, M. E. Anderson, S. Breit, and G. E. Trahey, "2-D motion estimation using two parallel receive beams," *IEEE Trans. Ultrason., Ferroelect., Freq. Contr.*, vol. 48, pp. 392–408, Mar. 2001.

[20] J. A. Jensen and P. Munk, "A new method for estimation of velocity vectors," *IEEE Trans. Ultrason., Ferroelect., Freq. Contr.*, vol. 45, pp. 837–851, May 1998.

[21] M. E. Anderson, "Multi-dimensional velocity estimation with ultrasound using spatial quadrature," *IEEE Trans. Ultrason., Ferroelect., Freq. Contr.*, vol. 45, pp. 852–861, May 1998.

[22] M. Calzolai, L. Capineri, A. Fort, L. Masotti, and M. Scabia, "A real time two-dimensional pulsed wave Doppler system," *Ultrasound Med. Biol.*, vol. 26, no. 1, pp. 121–131, 2000.

[23] L. Capineri, M. Scabia, and L. F. Masotti, "Vector Doppler: Spatial sampling analysis and presentation techniques for real-time systems," in *Proc. SPIE Med. Imaging Mtg.*, 2001, pp. 353–357.

[24] M. Berson, A. Roncin, and L. Pourcelot, "Compound scanning with an electrically steered beam," *Ultrason. Imag.*, vol. 3, pp. 303–308, 1981.

[25] S. K. Jespersen, J. E. Wilhjelm, and H. Sillesen, "Multi-angle compound imaging," *Ultrason. Imag.*, vol. 20, pp. 81–102, 1998.

[26] R. Entrekin, P. Jackson, J. R. Jago, and B. A. Porter, "Real time spatial compound imaging in breast ultrasound: Technology and early clinical experience," *MedicaMundi*, vol. 43, Sep. 1999.

[27] I. Céspedes, J. Ophir, and S. K. Alam, "The combined effect of signal decorrelation and random noise on the variance of time delay estimation," *IEEE Trans. Ultrason., Ferroelect., Freq. Contr.*, vol. 44, no. 1, pp. 220–225, 1997.

[28] R. Mallart and M. Fink, "Adaptative focusing in scattering media through sound speed inhomogeneities: The Van Cittert Zernike approach and focusing criteria," *J. Acoust. Soc. Amer.*, vol. 96, pp. 3721–3732, Dec. 1994.

[29] W. F. Walker and G. Trahey, "Speckle coherence and implications for adaptive imaging," *J. Acoust. Soc. Amer.*, vol. 101, pp. 1847–1858, Apr. 1997.

[30] S. Manneville, L. Sandrin, and M. Fink, "Investigating a stretched vortex with ultrafast 2-D ultrasonic speckle velocimetry," *Physics Fluids*, vol. 13, Jun. 2001.

[31] L. Sandrin, S. Manneville, and M. Fink, "Ultrafast two-dimensional ultrasonic speckle velocimetry: A tool in flow imaging," *Appl. Phys. Lett.*, vol. 78, pp. 1155–1558, Feb. 2001.

Mickaël Tanter was born in December 1970 in Paimpol, France. He received the ingeneer degree in electronics of SUPELEC in 1994. In 1999, he received the Ph.D. degree in physics (acoustics) from the University of Paris VII for his work on the application of time reversal to ultrasonic brain hyperthermia. He is now researcher in the National French Center of Science (C.N.R.S) and joined the laboratory Ondes et Acoustique at the Ecole Supérieure de Physique et de Chimie Industrielle de la Ville de Paris (ESPCI) in 2000. His current research interests include wave focusing techniques in heterogeneous media, medical ultrasonic imaging, ultrasonic brain imaging, shear wave propagation in soft tissues for cancer detection, ultrasonic therapy, nonlinear acoustics, and active noise control.

Jérémy Bercoff was born in August 1977 in Paris, France. He received the ingeneer degree from the Ecole Supérieure de Physique et de Chimie de Paris (ESPCI) with a specialization in physics (2001). In 1999, he worked at ATL Ultrasound, a Philips Medical System company based in Seattle, on the development of echographic systems. In 2000, he received his master degree at the Laboratoire Ondes et Acoustique in Paris. He is now achieving his Ph.D. at the Laboratoire Ondes et Acoustique, working on pulsed elastography, ultrafast imaging, and flow measurements.

Laurent Sandrin was born in Massy (France) on March 21, 1973. He received an Ing. degree from the Ecole Supérieure de Physique et de Chimie Industrielles de la Ville de Paris (ESPCI) with a specialization in physics in 1996. In 1994, he worked at the Sony Research Center in Yokohama (Japan) on large band-gap semiconductors for blue laser diodes. In 1996, he joined the Génie Physique Department of the Ecole Polytechnique de Montréal (Canada) to study the adhesion between metals (Al, Cu) and polymer films (PE, PET). In 2000, he received the Ph.D. at the Laboratoire Ondes & Acoustique in Paris, where he has worked on elastography as well as ultrafast imaging under the supervision of Mathias Fink. Since then, he has been working for Echosens, which specializes in developing medical equipment using ultrasound for elastographic measurements.

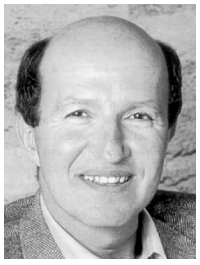

Mathias A. Fink received the diplome de Doctorat de 3$^{\text{ème}}$ cycle in solid state physics in 1970 and the Doctorat ès-Sciences degree in acoustics in 1978 from Paris University, France.

From 1981 to 1984, he was a professor of acoustics at Strasbourg University, France. Since 1984, he has been a professor of physics at Paris University (Denis Diderot), France. In 1990, he founded the Laboratoire Ondes et Acoustique at the Ecole Supérieure de Physique et de Chimie Industrielles de la Ville de Paris (ESPCI). In 1994, he was elected at the Institut Universitaire de France.

His current research interests include medical ultrasonic imaging, ultrasonic therapy, nondestructive testing, underwater acoustics, active control of sound and vibration, analogies between optics and acoustics, wave coherence in multiple scattering media, and time reversal in physics. He has developed different techniques in speckle reduction, wave focusing in inhomogeneous media, and in ultrasonic laser generation. He holds 20 patents, and he has published more than 220 articles.